Investigation of light propagation models to determine the optical properties of tissue from interstitial frequency domain fluence measurements

Heping Xu
Thomas J. Farrell
Michael S. Patterson
Juravinski Cancer Centre
Department of Medical Physics
699 Concession Street
Hamilton, Ontario L8V 5C2 Canada
    and
McMaster University
Department of Medical Physics and
    Applied Radiation Sciences
1280 Main Street West
Hamilton, Ontario L8S 4K1 Canada
E-mail: Heping.Xu@hrcc.on.ca

Abstract. Four models, standard diffusion approximation (SDA), single Monte Carlo (SMC), delta-P_1, and isotropic similarity (ISM), are developed and evaluated as forward calculation tools in the estimation of tissue optical properties. The inverse calculation uses the ratio of the fluences and phase difference at two locations close to an intensity modulated isotropic source to recover the reduced scattering coefficient μ_s' and the absorption coefficient μ_a. Diffusion theory allows recovery of optical properties (OPs) within 5% for media with $\mu_s'/\mu_a > 10$. The performance of the delta-P_1 model is similar to SDA, with limited enhanced accuracy. The collimation approximation may limit the use of the delta-P_1 model for spherical geometry, and/or the fluence may not be accurately calculated by this model. The SMC model is the best, recovering OPs within 10% regardless of the albedo. However, the necessary restriction of the searched OPs space is inconvenient. The performance of ISM is similar to that of diffusion theory for media with $\mu_s'/\mu_a > 10$, and better for $1 < \mu_s'/\mu_a < 10$, i.e., determines absorption within 5% and reduced scattering within 20%. In practice, satisfactory estimates (within 5 to 10%) can be achieved using SDA to recover μ_s' and ISM to recover μ_a for media with $\mu_s'/\mu_a > 5$. © 2006 Society of Photo-Optical Instrumentation Engineers.
[DOI: 10.1117/1.2241609]

Keywords: diffusion approximation; Monte Carlo simulation; delta-P_1; similarity relation; optical properties; tissue optics.

1 Introduction

A common goal in the application of light transport in medicine is to determine the optical properties (OPs) of tissue, typically the single scattering anisotropy factor, and the absorption and scattering coefficients. The relationship between measured physical quantities such as fluence, reflectance, or radiance and the OPs is established by linear transport theory (expressed by the Boltzmann equation). Generally speaking, methods for solving the transport equation fall into two categories: analytical and numerical techniques. For methods involving analytical techniques, the observed physical quantities cannot be explicitly expressed as elementary functions of OPs except for very simple cases. Hence, various approximations are employed to simplify the mathematics. Even with those simplifications, which render the explicit expression of observed physical quantities as functions of OPs, it is often the case that the reverse is not true, i.e., OPs cannot be explicitly expressed as elementary functions of observed physical quantities. A model that uses OPs as input to calculate the measured physical quantities is called a forward method or forward model. Once an appropriate forward model is chosen, a trial and error strategy is used to estimate OPs. Trial OPs are repeatedly put into the forward model to generate values of the observed quantities until preset criteria determine that values of the calculated quantities are sufficiently close to those measured, and the resultant OPs are deemed to be the true OPs. This entire process is called the inverse method or inverse model. Analytical methods are fast but cannot determine the measured quantities accurately in cases where the approximations used to obtain analytical expressions fail. Methods involving numerical techniques include Monte Carlo (MC) simulation, the finite element method (FEM),[1,2] and those borrowed from neutron transport theory such as the harmonic expansion method (P_N) and the discrete ordinates method. Although MC is accurate and can be applied to many cases where analytical methods fail, the associated computation burden often prevents its use as a forward model. Other numerical methods asymptotically approach true values of OPs if the spatio-temporal mesh is fine enough (FEM) or the number of expansion terms is large enough (P_N).

Following the previous two routes, a number of investigators developed algorithms to determine OPs quickly and ac-

Address all correspondence to Heping Xu, Medical Physics, Juravinski Cancer Centre, 699 Concession Street, Hamilton, Ontario L8V 5C2 Canada; Tel: 905–387–9711 ext 67152; Fax: 905–575–6337; E-mail: heping.xu@hrcc.on.ca

curately. They include standard diffusion approximation (SDA),[3,4] the delta-P_1 model,[5–9] path integral formalism,[10] MC,[11] and random walk method.[12,13] In practice, no method is superior in all cases, and the choice depends on the source and detector geometry, experimental measuring instruments, errors in OPs allowed, and range of OPs encountered.

This work focuses on comparing four models that are used inversely to determine OPs from frequency domain measurements. They are SDA, single Monte Carlo model (SMC), delta-P_1 model, and isotropic similarity model (ISM). The geometry is as follows. A source fiber with an isotropic tip, being regarded as an ideal point (for SDA, SMC, and ISM models) or a finite sphere (for delta-P_1 model), is embedded in an infinite homogeneous turbid medium. Two detectors are located in the medium. The perturbation of the fluence by the source and detector optical fibers was not accounted for in this work, but will be addressed in future experimental studies. The measured quantities are the ratio of the fluences and the phase difference at the two detectors at known distances. This particular geometry possesses clinical relevance in that it resembles the instrument configuration of interstitial treatment that may be clinically viable for photodynamic therapy (PDT) treatment of prostate tumors, breast lesions, or other tumors deeply seated in healthy tissues.

Although a turbid medium such as tissue usually is described by three interaction parameters, the anisotropy factor (g), the absorption (μ_a), and the scattering (μ_s) coefficients, it is often the case that use of two parameters, μ_a and the reduced scattering coefficient [$\mu_s' = (1-g)\mu_s$], are convenient and sufficiently accurate for characterization. Therefore, the OPs that were sought for this study are the absorption (μ_a) and reduced scattering (μ_s') coefficients.

Since the basic parameters of the diffusion model are μ_a and μ_s', the two measurements (fluence ratio and phase difference) can determine them uniquely.[14] In contrast, the SMC model and delta-P_1 model need three parameters (μ_a, μ_s, g) to complete forward calculations, and these cannot be uniquely determined by two measurements when the inverse calculation is performed. This situation is tempered by noting that fluence in media with high g ($g > 0.8$) such as tissue is relatively insensitive to the exact value of g.[15,16] In this work, *a priori* assumption of $g = 0.9$ will be used for SMC and delta-P_1 models.

The SDA model is mathematically simple and has proven to be effective when modeling light transport in tissues in many practical situations. Several authors have used measurements of phase and amplitude and the frequency domain diffusion equation to deduce the optical properties of turbid media.[17–19] However, it is well known that the model fails to give satisfactory results when 1. detecting positions are close to the source, 2. detecting positions are close to a boundary, 3. the absorption coefficient is comparable to the reduced scattering coefficient, and 4. the modulation frequency is too high. Hence, other methods have been proposed to overcome these limitations.

Monte Carlo simulation (MC) is considered a gold standard for solving light transport in turbid media. It can easily incorporate irregularly shaped boundaries, anisotropic sources and detector response, heterogeneity, etc. The main deterrent for MC to be used as a forward model is the computation

time. However, several papers have proposed a concept called single MC (or condensed MC) to get around the problem.[15,16,20–22] The basic idea is that the various scored quantities for different OPs are actually related to each other through scaling relationships. Hence MC needs to be run only once, and the scored quantities for a given set of OPs are obtained according to the scaling relationships. Graaff et al. showed that diffuse reflectance and transmittance could be obtained using single MC when a pencil beam was incident on a semi-infinite medium and a slab medium in steady state.[20] However, the reflectance and transmittance could only be obtained for various albedos while the total interaction coefficient had to remain unchanged. The work by Pifferi et al., who extended the method proposed by Kienle and Patterson (see later in this paragraph), showed the recovery of OPs in semi-infinite and slab geometry in a time-domain setup.[16] The work by Sassaroli et al. developed a MC procedure to study photon migration through highly scattering nonhomogeneous media.[21] Using two scaling relationships from astrophysics research, they could image defects embedded in a diffuse slab. In the work by Kienle and Patterson,[15] they calculated the time-resolved diffuse reflectance for a semi-infinite medium and indicated that diffuse reflectance in frequency domain can be obtained by Fourier transform of the time-domain data. The reference reflectance was obtained in a conservative medium, i.e., $\mu_a = 0$. Reflectance for nonconservative media was obtained using Beer's law [i.e., multiplying the reflectance by the factor $\exp(-\mu_a v t)$, where v and t are the speed of light in the medium and time, respectively]. The same logic can be applied to the estimation of fluence. This method assumes that reflectance (fluence) can be factored into two terms, which depend on the scattering and absorption coefficients, respectively. In the present study, the reference fluence was obtained in a nonconservative medium without using Beer's law. We show that the proposed method is equivalent to the method based on Beer's law, and computation time is similar for both methods.

Biological tissues typically scatter light predominantly in the forward direction. Hence an improvement over diffusion theory may result by including a delta function into the phase function, which can effectively account for the forward scattering that is not well described by diffusion theory. Usually, the phase function takes the form of the sum of a delta function and the Eddington phase function. When the resulting delta Eddington phase function is substituted into the transport equation, the radiance is naturally separated into two parts: the collided and uncollided components. The collided part can be calculated using the P_1 approximation similar to the mathematics used in the standard diffusion theory. The usefulness of this delta-P_1 approximation has been shown by several investigators.[5–9] Venugopalan et al. discussed the formulas in steady state for infinite and semi-infinite geometry with collimated beams of various profiles.[7,8] Hayakawa et al. used the delta-P_1 approximation as a forward model to recover OPs in turbid media in an infinite geometry.[23] The results showed that the delta-P_1 approximation estimated the irradiance and reflectance reasonably well close to the source for reduced single scattering albedo a' ranging from 0.248 to 0.997. It is also possible to recover the anisotropy factor using the delta-P_1 model. Most of the calculations to date, including

the inverse method based on delta-P_1 approximation, have been in the steady state, except the recent paper by You, Hayakawa, and Venugopalan, who did the forward calculation in the frequency domain. This work generalizes this approximation to the frequency domain and evaluates its ability to calculate fluence and phase.

It has long been recognized by investigators in light propagation modeling that the replacement of real optical coefficients by artificial, but equivalent, coefficients can offer advantages in radiation transport calculations. By equivalent, we mean that the observed quantities (fluence, reflectance, etc.) are invariant under the transformation of one set of OPs to another set of OPs. Wyman, Patterson, and Wilson proved that, strictly speaking, one radiance corresponds to one and only one set of OPs.[24] Hence any use of similarity relations invariably involves some kind of approximation. However, this does not detract from their usefulness. Van de Hulst and and Grossman showed that replacement of an anisotropic phase function by an equivalent isotropic phase function generally simplifies both analytical and numerical computation.[25] Wyman, Patterson, and Wilson showed that MC particle transport simulation could be accelerated by replacing μ_t with an equivalent smaller value.[26] Although the idea of similarity relations is appealing, several authors have found that it is not more useful than diffusion theory. Pronounced differences near the boundary between calculation results for anisotropic scattering and the isotropic scattering transport approximation have been observed even if the reduced single scattering albedo is low.[27] Graaff et al. showed that the similarity relation holds well in turbid media with a value of g in the range of 0.9 to 1 in an unbound medium with a broad parallel beam serving as a source.[28] Van de Hulst and Graaff later provided a sound basis for these observations.[29] In this work, we ascertain the validity of the similarity relations for calculating fluence in the frequency domain in infinite geometry.

2 Theory

This section discusses the theoretical aspects of the four models: diffusion model (SDA), single Monte Carlo simulation (SMC), delta-P_1 model, and isotropic similarity model (ISM), and the associated inversion schemes using these models.

2.1 Diffusion Model

The diffusion equation for the fluence rate (strictly speaking, the diffuse photon density wave, but we use the term fluence interchangeably) in the frequency domain reads:

$$(\nabla^2 - k_d^2)\varphi(\vec{r},\omega) = -S(\vec{r},\omega), \qquad (1)$$

where k_d is the complex effective attenuation coefficient

$$k_d = [(\mu_a - i\omega/v)/D]^{1/2}$$

with $\mathrm{Re}(k_d) > 0$, v is the light speed in tissue, ω is the product of 2π and modulation frequency, D is the diffusion coefficient equal to $1/[3(\mu_s' + \mu_a)]$, and $\vec{r}$ is the position relative to the source. When the source term $S(\vec{r},\omega)$ is a sinusoidally modulated isotropic point source with strength S_0, the solution is given by:

$$\varphi(\vec{r},\omega) = \frac{S_0 \exp(-k_d r)}{4\pi D r}. \qquad (2)$$

Note that $\varphi(\vec{r},\omega)$ is complex, so that the phase of the AC fluence relative to the source $S(\vec{r},\omega)$ is given by

$$\theta = \tan^{-1}[\mathrm{Im}(\varphi)/\mathrm{Re}(\varphi)], \qquad (3)$$

and the amplitude A is

$$A = [\mathrm{Re}^2(\varphi) + \mathrm{Im}^2(\varphi)]^{1/2}. \qquad (4)$$

The steady-state solution is obtained by setting the modulation frequency to zero.

2.2 Single Monte Carlo Simulation

For the basics of Monte Carlo simulation, refer to the paper by Jacques and Wang.[11] This section shows how the fluences resulting from different OPs are related each other and what scored quantities are needed.

To exploit the spherical symmetry of the geometry, the scoring volumes are concentric shells centered at the origin. The fluence as a function of time and radius then is proportional to the photon weights deposited in the shell, as expressed by the equation:

$$\phi(t,r) = \frac{1}{\mu_a} \frac{W_{abs}(t,r)}{\Delta V}, \qquad (5)$$

where μ_a is the absorption coefficient, W_{abs} is the absorbed photon weight in ΔV, and ΔV is the differential volume $4\pi r^2 dr$. Now we need to calculate W_{abs}. In the Monte Carlo simulation, if N photons were launched at the origin, the total absorbed weight is:

$$W_{abs}(t,r) = \frac{1}{N}\sum_{k=1}^{P}\left(\frac{\mu_s}{\mu_t}\right)^{n_k}\left(\frac{\mu_a}{\mu_t}\right), \qquad (6)$$

where P is the total number of launched photons that interact with the medium at the space-time point (t,r), n_k is the number of scattering events the photon suffers before it reaches the space-time point (t,r), and μ_s, μ_a, and μ_t are the scattering, absorption, and total interaction coefficients, respectively. It should be noted that P and n_k are functions of space-time. The fluence can be calculated by substituting W_{abs} into Eq. (5):

$$\phi(t,r) = \frac{1}{\Delta V \cdot \mu_t} \cdot \frac{1}{N}\sum_{k=1}^{P}\left(\frac{\mu_s}{\mu_t}\right)^{n_k}. \qquad (7)$$

Strictly speaking, n_k is not the same for every photon launched at the origin, but if we assume that n_k can be replaced by the average $\bar{n}$, we get:

$$\bar{n} = \frac{1}{P}\sum_{k=1}^{P} n_k, \qquad (8)$$

$$\phi(t,r) = \frac{1}{\Delta V \cdot \mu_t} \frac{P}{N} \left(\frac{\mu_s}{\mu_t} \right)^{\bar{n}}. \tag{9}$$

In Eq. (9) the space-time dependent variables P and $\bar{n}$ can be obtained by using Monte Carlo simulation only once. Fluences due to different values of μ_a and μ_s can be obtained from Eq. (9) as follows. In Monte Carlo simulation, the pathlength (equivalently the time) a photon travels is generated by a random number according to $-1/\mu_t \ln(x)$, where x is a random number uniformly distributed between 0 and 1. This shows that pathlengths (or time) are linear with respect to $1/\mu_t$. This prompts us to think that any variable associated with time or pathlengths must be scaled accordingly, which leads to the final result for calculating fluence for any set of absorption and scattering coefficients:

$$\phi(t,r) = \phi\left(\frac{\mu_{tn}}{\mu_t} t, \frac{\mu_{tn}}{\mu_t} r \right) = \left(\frac{\mu_{tn}}{\mu_t} \right)^4 \cdot \frac{1}{\Delta V \cdot \mu_{tn} \cdot N} \cdot P\left(\frac{\mu_{tn}}{\mu_t} t, \frac{\mu_{tn}}{\mu_t} r \right)$$
$$\cdot \left(\frac{\mu_{sn}}{\mu_{tn}} \right)^{\bar{n}\left(\frac{\mu_{tn}}{\mu_t} t, \frac{\mu_{tn}}{\mu_t} r \right)}, \tag{10}$$

where n in the subscript denotes the new set of optical properties, and the prefactor with the power of four contains both spatial and temporal dimensions because of the scoring geometry, and because we are dealing with the fluence rate.

In Eq. (9), the fluence rate is proportional to the total number of interactions modified by the weight related to the albedo. The accuracy of this algorithm depends on the replacement of a series of numbers n_k for different photons by one number $\bar{n}$. MC simulation is a statistical technique, and the probability of one photon arriving at (t,r) is obtained by sampling N identical photons, each of them contributing to the sought probability with equal importance. Mathematically,

$$X = \frac{1}{N} \sum_{i=1}^{N} X_i,$$

where X denotes the sought probability for one photon, and X_i denotes the probability for the simulated ith photon. The central limit theorem tells us that X converges to the normal distribution regardless of the shape of individual distributions X_i, provided N is sufficiently large. Hence we can assume that the interaction history for a photon reaching (t,r) follows a normal distribution. The simulation data show that the width is usually small, so that the spread exerted by the medium is negligible. The transition from Eq. (7) to Eq. (9) implies that we can use one universal number of interactions for all photons. The determination of this universal number still requires Monte Carlo simulation. The advantage of this replacement is that the albedo is decoupled from the number of interactions, and the single Monte Carlo simulation can be scaled as a result of this decoupling.

Equation (9) indicates that the fluence rate is related to the photon interaction density (P/N) and the scattering history $\bar{n}$. The photon interaction density is a measure of how often a photon visits a particular differential volume in a particular time interval. The proportionality of this quantity to the fluence rate is reasonable, since we expect that the fluence rate at a position will be larger if photons have more chances to "hit" that position. Scattering history is a measure of how many scatterings a photon undergoes just before it reaches a particular space-time point. It is clear that more scatterings will certainly reduce the fluence rate at a position, because fewer photons will arrive at that position. The quantitative relationship between the fluence rate and the scattering history is, however, not linear but is given by a power law, with the albedo coming into play as the base. The previous analysis shows that determining the fluence rate is equivalent to determining the photon interaction density and scattering history. This equivalence can also be applied to other geometries such as semi-infinite and slab geometries.

Furthermore, we point out that $\bar{n}$ is independent of the position for a given value of time and is proportional to time, with the proportionality constant being the product of the scattering coefficient (μ_s) and the speed of light (v) in the medium. The reason is straightforward. The distance traversed by a photon between two successive scatterings is $v \cdot \Delta t$, where Δt is the time elapsed between the two scatterings. The total distance traveled is vt after $\bar{n}$ scatterings. On average, that distance is $\bar{n}$ divided by μ_s. Combining the two equations results in the statement at the beginning of this paragraph. This observation offers convenience in calculating $\bar{n}$ in inverse computation, since one simple equation allows us to get the scattering history for arbitrary position and time, and it is not necessary to parameterize the SMC data.

An alternative method follows the paper by Kienle and Patterson.[15] From the results of a MC simulation performed for a conservative medium characterized by μ_{sr}, fluence can be obtained for arbitrary μ_s and μ_a using Beer's law and scaling relations:

$$\phi(t,r) = \left(\frac{\mu_s}{\mu_{sr}} \right)^3 \phi_r \left(t \frac{\mu_s}{\mu_{sr}}, r \frac{\mu_s}{\mu_{sr}} \right) \exp(-\mu_a vt). \tag{11}$$

The scaling constant here is the scattering coefficient instead of the total interaction coefficient. Comparing Eq. (11) with Eq. (10), it can be seen that photon interaction density is equivalent to the reference fluence in a conservative medium, and the exponential decay in the form of Beer's law is equivalent to the scattering history.

The proposed method, which has two parameters to fit, looks more complicated than the previous method,[15] which has one parameter to fit the fluence rate data. Actually, the computation burden for both methods is essentially the same, because the proposed method does not need a look-up table for calculating scattering history, which is just the product of light speed and travel time. Look-up tables must be built for interaction density in the proposed method, and fluence rate in conservative medium in the previous method.[15]

Time-resolved data are transformed to frequency domain data using Fourier transform as shown in Appendix A in Sec. 5.

2.3 Delta-P_1 Model

This section first briefly reviews the derivation following the paper by Venugopalan, You, and Tromberg.[7] This is extended to obtain the exact solution for a finite spherical source, and it is shown that the previously obtained analytical solution[7] is approximate and valid only when the dimension of the source is small. The collimation approximation in the derivation is

also discussed. The solution has been generalized to the frequency domain (FD), where the functional form resembles its steady-state solution.

2.3.1 Delta-Eddington phase function

As noted earlier, the scattering phase function is replaced by the delta-Eddington phase function, which takes the form:

$$P_{\delta-E}(\hat{s},\hat{s}') = \frac{1}{4\pi}\{(1-f)[1+3g^*\cdot(\hat{s}\cdot\hat{s}')] + 2f\delta(1-\hat{s}\cdot\hat{s}')\},$$

(12)

where f is the fraction of light directly scattered forward and is between 0 and l, and g^* is the scattering anisotropy factor for the Eddington phase function and is a counterpart to g in the Henyey-Greenstein phase function. The relationship between them can be obtained by matching the first and second moments of the two phase functions, as the paper by Wiscombe[30] indicated. Substituting the delta-Eddington phase function [Eq. (12)] into the well-known Boltzmann equation:

$$\frac{1}{v}\frac{\partial L(\vec{r},\hat{s},t)}{\partial t} + \hat{s}\cdot\nabla L(\vec{r},\hat{s},t) + \mu_t L(\vec{r},\hat{s},t)$$

$$= \mu_s\int_{4\pi} L(\vec{r},\hat{s}',t)p(\hat{s},\hat{s}')d\Omega + S(\vec{r},\hat{s},t),$$

(13)

results in:

$$\frac{1}{v}\frac{\partial L(\vec{r},\hat{s},t)}{\partial t} + \hat{s}\cdot\nabla L(\vec{r},\hat{s},t) + \mu_t^* L(\vec{r},\hat{s},t)$$

$$= \mu_s^*\int_{4\pi} L(\vec{r},\hat{s}',t)p_E(\hat{s},\hat{s}')d\Omega + S(\vec{r},\hat{s},t),$$

(14)

where $\mu_s^* = \mu_s(l-f)$, $\mu_t^* = \mu_a + \mu_s^*$, and $p_E(\hat{s},\hat{s}')$ is the Eddington phase function given by:

$$p_E(\hat{s},\hat{s}') = \frac{1}{4\pi}[1+3g^*\cdot(\hat{s}\cdot\hat{s}')].$$

(15)

2.3.2 Decomposition of radiance

The radiance is approximated by the sum of two parts: the uncollided component (pointed in $\hat{s}_0$, the unit vector collinear with the direction of the uncollided component), denoted by $L_c(\vec{r},\hat{s},t)$ and the diffusion component denoted by $L_d(\vec{r},\hat{s},t)$. The uncollided component can be written as:

$$L_c(\vec{r},\hat{s},t) = \frac{1}{2\pi}P(\vec{r},\hat{s},t)\delta(1-\hat{s}\cdot\hat{s}_0),$$

(16)

where $P(\vec{r},\hat{s},t)$ is the characteristic "irradiance" for the source, i.e., the integral of the uncollided component $L_c(\vec{r},\hat{s},t)$ over 4π. Here $P(\vec{r},\hat{s},t)$ refers to a general source.

The diffusion component satisfies the following equation:

$$\frac{1}{v}\frac{\partial L_d(\vec{r},\hat{s},t)}{\partial t} + \hat{s}\cdot\nabla L_d(\vec{r},\hat{s},t) + \mu_t^* L_d(\vec{r},\hat{s},t)$$

$$= \mu_s^*\int_{4\pi} L_d(\vec{r},\hat{s}',t)p_E(\hat{s},\hat{s}')d\Omega + \mu_s^*P(\vec{r},\hat{s}_0,t)p_E(\hat{s},\hat{s}')$$

$$- \frac{1}{2\pi v}\frac{\partial P(\vec{r},\hat{s},t)}{\partial t}\delta(1-\hat{s}\cdot\hat{s}_0).$$

(17)

It is worthwhile to note that the following approximation has been used in the derivation of the previous equation:

$$\hat{s}\cdot\nabla L_c(\vec{r},\hat{s},t) = -\mu_t^* L_c(\vec{r},\hat{s},t).$$

(18)

This is strictly correct for exponentially decreasing uncollided radiance, but not for the uncollided radiance $L_c(\vec{r},\hat{s},t)$ given by:

$$L_c(\vec{r},\hat{s},t) = P(\vec{r},\hat{s},t)\frac{\delta(1-\hat{s}\cdot\hat{r})}{2\pi}\exp(-i\omega t)$$

$$= \frac{\exp[-\mu_t^*(r-r_0)]}{4\pi r^2}\frac{\delta(1-\hat{s}\cdot\hat{r})}{2\pi}\exp(-i\omega t),$$

(19)

where r_0 is the radius of the source, and $\hat{r}$ is $\vec{r}/r$. The gradient of this radiance projected in $\hat{r}$ is $-(\mu_t^*+2/r)L_c(\vec{r},\hat{s},t)$. Hence, Eq. (18) is valid for $r\gg 1/(2\mu_t^*)$.

2.3.3 Boundary condition

To solve the integro-differential equation [Eq. (17)] concerning the diffuse part, the boundary conditions must be specified. In our geometry, a spherical source with radius of r_0 is embedded the medium at the origin. We quote the results of the boundary conditions obtained by Venugopalan, You, and Tronberg:[7]

$$\varphi_d(\vec{r}) - \left(\frac{2Ahv}{2v-3i\omega h}\right)\hat{r}\cdot\nabla\varphi_d(\vec{r})$$

$$= \frac{-6Ahv}{2v-3i\omega h}\left(g^*\mu_s^* + \frac{i\omega}{v}\right)\frac{1}{4\pi r_0^2},$$

(20)

$$\varphi_d(r) \to 0 \quad \text{for } r \to \infty,$$

(21)

where φ_d is the diffuse fluence, $h=1/\mu_t'$, $A=(1+R_2)/(1-R_1)$, $R_1=2\int_0^1 r_F(\nu_0)\nu_0 d\nu_0$, and $R_2=3\int_0^1 r_F(\nu_0)\nu_0^2 d\nu_0$. ν_0 is the cosine of the angle between the photon direction and surface normal and $r_F(\nu_0)$ is the Fresnel coefficient. Boundary conditions for the steady state are obtained by setting ω to zero.

2.3.4 Mathematical equations

To summarize the previous results, the physical problem reduces to solving the following equation,

$$\left[\nabla^2 - 3\mu_a\mu_t' + \frac{3\omega^2}{v^2} + \frac{3(\mu_a + \mu_t')}{v}i\omega\right]\varphi_d(\vec{r},\omega)$$

$$= \left[-3\mu_s^*\mu_t' + \frac{3\omega^2}{v^2} - \frac{3i\omega(\mu_t' - \mu_s^*)}{v}\right]P(\vec{r},\hat{s}_0,\omega)$$

$$+ 3\left(g^*\mu_s^* + \frac{i\omega}{v}\right)\hat{s}_0 \cdot \nabla P(\vec{r},\hat{s}_0,\omega),\qquad(22)$$

with Eqs. (20) and (21) as boundary conditions. The unit isotropic source $P(\vec{r},\hat{s},\omega)$ is given by Eq. (19).

2.3.5 Solution of the equations

First we obtain the exact solution for the steady-state equation. We omit the detailed calculation here, but it may be found in Appendix B in Sec. 6. The steady-state solution is as follows:

$$\varphi_d(r) = \varphi_{d1}(r) + \varphi_{d2}(r),\qquad(23)$$

where

$$\varphi_{d1}(r) = \frac{3\mu_s^*(\mu_t^* + g^*\mu_a)\exp(\mu_t^*r_0)}{8\pi\mu_{\mathrm{eff}}r}\left\{\left[E_1(\mu_t^*r_0 - \mu_{\mathrm{eff}}r_0)\right.\right.$$

$$- E_1(\mu_t^*r - \mu_{\mathrm{eff}}r) - E_1(\mu_t^*r_0 + \mu_{\mathrm{eff}}r_0)$$

$$\left.- \frac{2g^*\sinh(\mu_{\mathrm{eff}}r_0)}{r_0(\mu_t^* + g^*\mu_a)\exp(\mu_t^*r_0)}\right]\exp(-\mu_{\mathrm{eff}}r)$$

$$+ E_1(\mu_t^*r + \mu_{\mathrm{eff}}r)\exp(\mu_{\mathrm{eff}}r)\bigg\},\qquad(24)$$

and

$$\varphi_{d2}(r) = -\widetilde{C}_0\frac{3\mu_s^*(\mu_t^* + g^*\mu_a)}{8\mu_{\mathrm{eff}}r}$$

$$\times\exp(\mu_t^*r_0 - \mu_{\mathrm{eff}}r)E_1(\mu_t^*r_0 + \mu_{\mathrm{eff}}r_0)$$

$$+ \widetilde{C}_0\frac{3\mu_s^*g^*}{8\mu_{\mathrm{eff}}rr_0}\exp(-\mu_{\mathrm{eff}}r - \mu_{\mathrm{eff}}r_0).\qquad(25)$$

Compared to the results obtained previously by Venugopalan, You, and Tromberg,[7] our solution includes an extra term. This term comes from Green's function. It is shown in Sec. 3 that the contribution of this extra term is negligibly small unless the source dimension is large. This also demonstrates that Green's function for an infinite medium is a good approximation for Green's function in our semi-infinite spherical geometry in steady state, as long as the source is small. We use this approximation in the frequency domain to simplify the calculation.

Following the same procedure used in steady state, we obtain the diffuse component of the fluence in the frequency domain:

$$\varphi_d(r,\omega) = \frac{3[\mu_s^*(\mu_t^* + g^*\mu_a) - \omega^2/v^2 + i\omega(\mu_a + \mu_t')/v]\exp(\mu_t^*r_0)}{8\pi kr}\{[E_1(\mu_t^*r_0 - kr_0) - E_1(\mu_t^*r - kr) - E_1(\mu_t^*r_0 + kr_0)]\exp(-kr)$$

$$+ E_1(\mu_t^*r + kr)\exp(kr)\} - \frac{3(g^*\mu_s^* + i\omega/v)\sinh(kr_0)}{4\pi krr_0}\exp(-kr),\qquad(26)$$

where $k = \{3[\mu_a\mu_t' - \omega^2/v^2 - i\omega(\mu_a + \mu_t')/v]\}^{1/2}$ with $\mathrm{Re}(k) > 0$.

The calculation involves complex numbers and can easily be dealt with using MatLab. The magnitude and phase of the fluence can then be calculated from the complex fluence $\varphi_d(r,\omega)$. The uncollided component in the frequency domain is the Fourier transform of the integration of Eq. (16) over 4π:

$$\varphi_c(r,\omega) = \frac{\exp[-\mu_t^*(r - r_0)]}{4\pi r^2}\exp\left[i\frac{\omega}{v}(r - r_0)\right].\qquad(27)$$

The total fluence is the sum of the uncollided component and diffuse component.

2.4 Isotropic Similarity Model

We assume that the fluence distribution is invariant when a triplet (μ_a,μ_s,g) is replaced by another triplet (μ_a^n,μ_s^n,g^n), provided the first-order similarity relation holds:[26]

$$\mu_a[\mu_a + (1 - g)\mu_s] = \mu_a^n[\mu_a^n + (1 - g^n)\mu_s^n].\qquad(28)$$

In our case, to further simplify the calculation, the absorption coefficient was chosen to be fixed and g^n was chosen to be zero. Hence we replace a highly forward scattering medium by an equivalent isotropic scattering medium. The basis of this assumption is purely empirical and is discussed in Sec. 3.

Consider the real medium with OPs (μ_a,μ_s,g) replaced by the equivalent medium with OPs $(\mu_a,\mu_s',0)$, where $\mu_s' = (1 - g)\mu_s$. The transport equation for the equivalent medium in the frequency domain is given by:

$$\hat{s} \cdot \nabla\Psi(\vec{r},\hat{s}) + \widetilde{\mu}_t\Psi(\vec{r},\hat{s}) = \frac{\mu_s'}{4\pi}\varphi(\vec{r}) + S(\vec{r}),\qquad(29)$$

where the isotropic phase function defined as $p(\hat{s},\hat{s}') = 1/4\pi$ has been used, $\widetilde{\mu}_t = \mu_t' - i\omega/v$, and $\varphi(\vec{r}) = \int_{4\pi}\Psi(\vec{r},\hat{s})d\hat{s}$ is the fluence. The source term is $S(\vec{r}) = \delta(\vec{r})/4\pi$. First, we get the steady-state solution for Eq. (29) by setting the frequency to

zero. The solution has been found by Case, de Hoffmann, and Placzek:[31]

$$\varphi(r) = \frac{\mu_t'}{4\pi r}\left[\frac{\partial k_0^2}{\partial c}\exp(-a_0\mu_t' r) + \int_0^1 g(c,\xi)\exp(-\mu_t' r/\xi)\frac{d\xi}{\xi^2}\right], \quad (30)$$

where c is the albedo, defined as μ_s'/μ_t'; the real parameter a_0 is the root of the equation $c = a_0/\tanh^{-1}a_0$; the parameter k_0 is imaginary and is defined as $k_0 = ia_0$; and the functional form of $g(c,\xi)$ is $1/[(1 - c\xi\tanh^{-1}\xi)^2 + (\pi c\xi/2)^2]$.

The solution for the frequency domain is more complicated and has not been published to our knowledge. We derive the solution by making use of reasonable approximations for the mathematics to be tractable. We first obtain a particular solution $\varphi_p(\vec{r})$ of Eq. (29).

$$\varphi_p(\vec{r}) = \int [\mu_s'\varphi(\vec{r}') + \delta(\vec{r}')]\frac{\exp(-\tilde{\mu}_t|\vec{r} - \vec{r}'|)}{4\pi|\vec{r} - \vec{r}'|^2}d^3\vec{r}'. \quad (31)$$

Taking the Fourier transform of the previous equation with respect to $\vec{r}$, we can express the fluence in spatial frequency space explicitly:

$$\varphi_p(\vec{k}) = \frac{\tan^{-1}(k/\tilde{\mu}_t)}{k - \mu_s'\tan^{-1}(k/\tilde{\mu}_t)}, \quad (32)$$

where k is the magnitude of $\vec{k}$. The inverse Fourier transform yields the fluence in position space:

$$\varphi_p(\vec{r}) = \frac{1}{(2\pi)^3}\int \varphi_p(\vec{k})\exp(i\vec{k}\cdot\vec{r})d^3\vec{k}. \quad (33)$$

We exploit the following approximation to reduce the integral in Eq. (33) to a simpler form. If we are dealing with a turbid medium with a reduced total interaction coefficient much larger than the modulation frequency divided by the light speed in the medium, then the inverse tangent function in Eq. (32) can be Taylor expanded with respect to k. This is reasonable, since the reduced total interaction coefficient in biological tissues is typically larger than 0.1 mm^{-1} and the modulation frequency we are using is around 100 MHz. The relationship that $\mu_t' \gg \omega/v$ is readily satisfied. Physically, this approximation states that the frequency of photon interaction with the medium is much greater than the modulation frequency. Hence, we have:

$$\tan^{-1}\left(\frac{k}{\tilde{\mu}_t}\right) = \tan^{-1}\left(\frac{k}{\mu_t'} + \frac{i\omega k}{\mu_t'^2 v}\right)$$

$$= \tan^{-1}\left(\frac{k}{\mu_t'}\right) + \frac{i\omega k}{\mu_t'^2 v}\cdot\frac{1}{1 + (k/\mu_t')^2} + O(\omega^2). \quad (34)$$

Substituting the previous expression into Eq. (33) allows us to get the approximate fluence:

$$\varphi_p(\vec{k}) = \frac{M + iN + O(\omega^2)}{Q - iN\mu_s' + O(\omega^2)} \approx \frac{M}{Q} + i\frac{N}{Q^2} + O(\omega^2), \quad (35)$$

where

$$M = \frac{1}{k}\tan^{-1}\left(\frac{k}{\mu_t'}\right), \quad N = \frac{\omega}{v}\cdot\frac{1}{k^2 + \mu_t'^2},$$

and $Q = 1 - M\mu_s'$. It can be seen that the real part of $\varphi_p(\vec{k})$ is the same as the fluence for the steady-state situation. Hence we need to calculate only the imaginary part of $\varphi_p(\vec{k})$. The imaginary part of the fluence in position space is expressed as follows, after changing k into the dimensionless quantity k' (equal to k/μ_t'):

$$\text{Im}[\varphi_p(r)] = \frac{1}{2\pi r}\cdot\frac{\omega}{v}\cdot F(r), \quad (36)$$

where

$$F(r) = \frac{1}{2\pi i}\int_{-\infty}^{+\infty}\frac{k'}{k'^2 + 1}\cdot\frac{\exp(ik'\mu_t' r)}{[1 - (c/k')\cdot\tan^{-1}k']^2}dk'. \quad (37)$$

Detailed evaluation of this integral is included in Appendix C in Sec. 7. The general solution that satisfies the boundary conditions (i.e., fluence vanishes at infinity) is proved to be equal to the particular solution in the book by Case, de Hoffmann, and Placzek.[31]

The approximations employed in deriving Eqs. (34) and (35) need further comment. In Eq. (34) second- and higher-order terms are lumped into $O(\omega^2)$, which really is $O(T\omega^2)$, where T is a function of spatial frequency, optical properties, and speed of light. It can be shown that this coefficient T is substantially less than the coefficient in the first-order term for all k, provided $\mu_t' \gg \omega/v$. Thus the approximation used here is reasonable. The validity of the approximation used in Eq. (35) becomes less predictable, since other coefficients, which are functions of spatial frequency and optical properties, contribute to the coefficient of ω^2, and due to the unknown magnitude of that coefficient, ω^2 may not be small compared to the first-order term. Hence Eq. (36), resulting from the prior approximations, may not be correct for certain values of OPs. An alternative method to obtain the fluence and phase is to evaluate the Fourier-type integral [Eq. (33)] directly in the complex domain using a proper numerical method. We performed evaluations using the double exponential formula.[32] These two methods are compared in Sec. 3.

2.5 Inversion Scheme

The fluence and phase data were generated using our conventional MC program in steady state and in the frequency domain with modulation frequency of 100 MHz. The geometry in the simulation program was the same as that described in the Introduction in Sec. 1. This program allowed for anisotropic light scattering by utilizing the Henyey-Greenstein (HG) phase function. Isotropic light scattering can also be simulated using the same HG phase function by setting the anisotropy factor to zero. For the source, light was emitted in all directions with equal probability (isotropic). It was a point
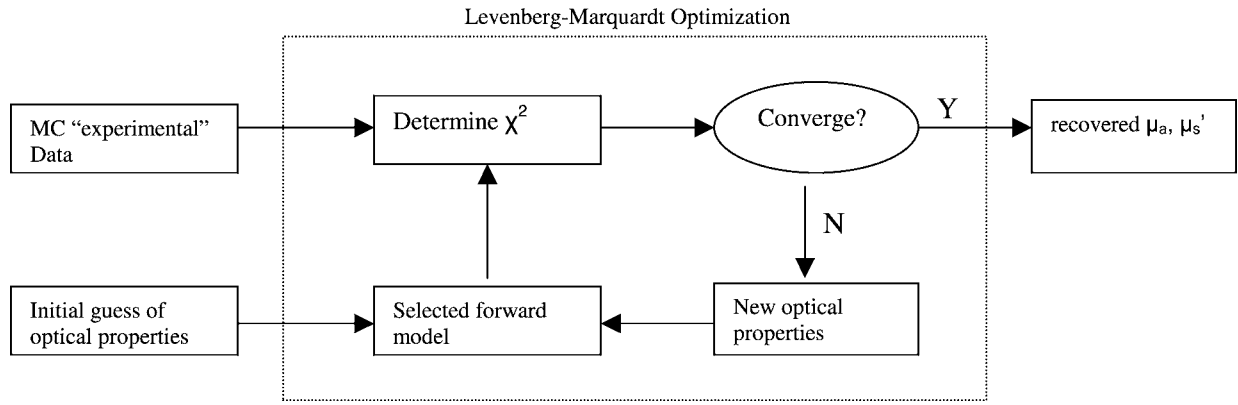
Levenberg-Marquardt Optimization

Fig. 1 Schematic representation of generic nonlinear optimization algorithm.

object except for the delta-P_1 model, where the light emitting tip was spherical, and the index of refraction (1.33) of the tip was assumed to be matched to the medium. The radial distance ranged from 0.1 to 100 mm with an increment of 0.1 mm for scoring.

Figure 1 shows the generic inversion scheme. Fluence and/or phase data and trial OPs were used to calculate χ^2 using the selected forward model. The trial OPs were adjusted until $|(\chi^2_{prev} - \chi^2_{cur})/\chi^2_{cur}| < 10^{-15}$, where χ^2_{cur} and χ^2_{prev} refer to the values for the current and previous iterations. The value of 10^{-15} was selected because further reduction yielded insignificant change in estimated OPs. χ^2 is defined as:

$$\chi^2 = \left(\frac{R_m - R_c}{\delta R_m}\right)^2 + \left(\frac{\phi_m - \phi_c}{\delta \phi_m}\right)^2,$$

where R (ϕ) is the ratio of the fluences (phase difference) at two known distances; δR ($\delta\phi$) is the intrinsic fluctuation of the MC simulation, or the appropriate values of the standard deviation of the fluence and phase when the noise was added to test robustness of the algorithm; and m and c denote measured and calculated, respectively. The Levenberg-Marquardt optimization algorithm[33] was chosen to minimize χ^2.

In SMC, the photon interaction density (P/N) and scattering history ($\bar{n}$) were obtained by MC code with OPs $(\mu_a, \mu_s, g) = (0.01 \text{ mm}^{-1}, 10 \text{ mm}^{-1}, 0.9)$. The raw MC data are discrete in position and time. The discreteness has to be extrapolated to continuity before the inverse algorithm can be applied, otherwise the inversion will terminate prematurely with totally unacceptable estimated optical properties. In other words, data in both $\bar{n}$ and P have to be parameterized. The scattering history is independent of position and is linearly related to time. The proportionality constant, although in principle equal to the scattering coefficient times the light speed in the medium as discussed in Sec. 2 was found by using linear regression to be 2.1457/sec. The calculation of interaction density is more subtle in that it does not appear to be a simple mathematical function of space and time. A practical way to solve this problem is to fit the MC generated interaction density as a function of time to a 20-deg polynomial at each fixed position. The data for other points can be interpolated using the MatLab function *polyval*. Although in principle SMC can use any optical properties to calculate phase and fluence at

any position, the reduction of dynamic range due to the scaling effects limits its use for large optical coefficients at large distances. Hence a limit of $\mu_t = 25 \text{ mm}^{-1}$ was set to prevent the algorithm from searching the parameter space where large coefficients lie. For low total interaction coefficients (around 1.00 mm^{-1}), the data developed previously were not used, since the scaling factor of 10 severely reduces the valid range of the fitting algorithm. Hence a dataset using 1.00 mm^{-1} as a reference total interaction coefficient was developed, following the same procedure described before.

3 Results and Discussion

3.1 Verification of Single Monte Carlo

The verification of the theory of SMC was performed in two steps: validation of interaction history and that of scaling relations. To validate the replacement of a series n_k by one universal number $\bar{n}$, we chose four space-time points at different distances from the source, as shown in Table 1. We tracked 30,000 photons for each point to get sufficient statistics. The arithmetic mean number of interactions before a photon reaches the chosen point is virtually identical to the fitted Gaussian mean. The spread measured by σ_{gau} decreases steadily to less than 5%. The reduced χ^2 is between 0.64 and 2, indicating it is highly likely that n_k is normally distributed, although a small deviation occurs for a position very close to the source. Satisfactory agreement was also seen when the

Table 1 Data for testing universality of scattering history $\bar{n}$. θ_{ari} and θ_{gau} denotes the arithmetic and Gaussian mean, respectively. χ^2/ν denotes the reduced chi squared.

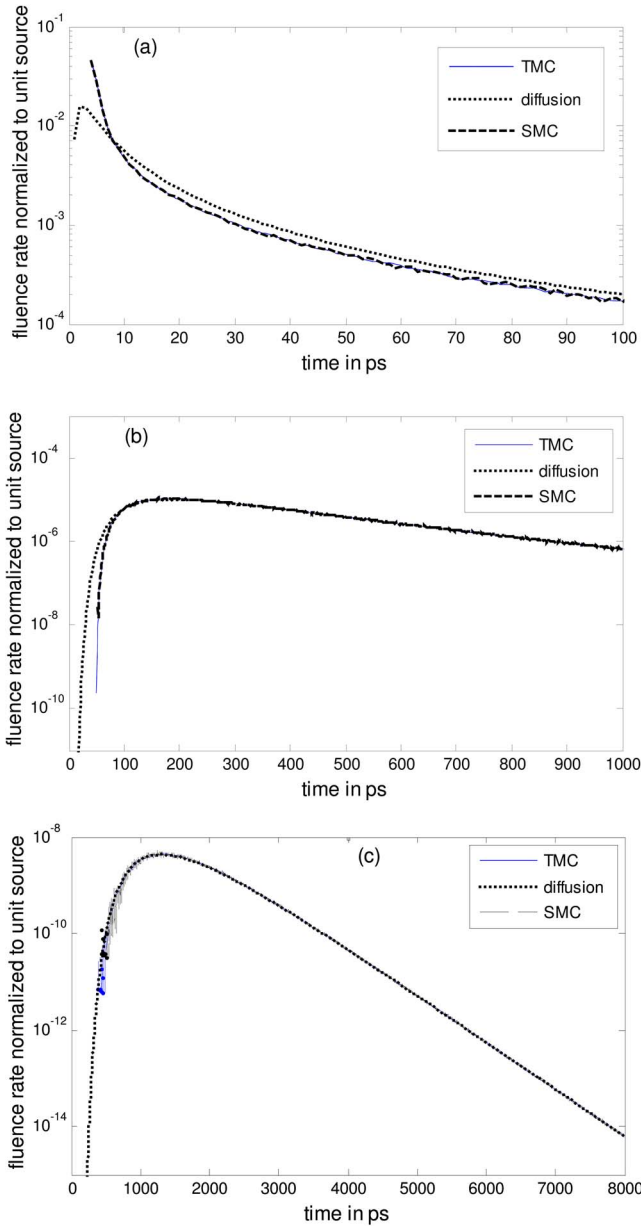| Position (mm)	Time (ps)	θ_{ari}	θ_{gau}	σ_{gau}	χ^2/ν
0.5	10	24.l	24.2	4.7	2.08
5	100	216.4	216.4	14.7	0.8054
10	500	1074.9	1074.9	32.2	0.9595
20	800	1717.2	1717.2	41.5	0.6450

Fig. 2 Comparison of the fluence rates in time domain obtained from diffusion model (dotted line), TMC (solid line), and SMC (dashed line) at distances of (a) 1, (b) 10, and (c) 40 mm from the source for μ_a =0.01 mm^{-1}, μ_s'=1.00 mm^{-1}. Note that time scale for short distance is reduced to emphasize the difference in fluence rates at an early time.

corresponding frequency histograms were drawn compared to the fitted curves (not shown here in the interest of space).

To test the scaling relationships, we chose three representative points at 1, 10, and 40 mm from the source. Figure 2 shows the comparison between the fluence rates in the time domain with μ_a=0.01 mm^{-1} and μ_s'=1.00 mm^{-1} using traditional Monte Carlo (TMC) simulation and SMC at all three distances. Also shown is the fluence rate calculated by diffusion theory. In Figs. 2(a) and 2(b), where the points are not far from the source, the diffusion theory differs from SMC and TMC at early times, while SMC and TMC are essentially

Table 2 Combinations of optical properties.

$\mu_s'(1/\text{mm})$	1.00 (ref)	3.00 (high)	0.5 (low)	4.00 (high)	0.40 (low)
$\mu_a(1/\text{mm})$	0.01 (ref)	0.10 (high)	0.2 (high)	0.001 (low)	0.001 (low)

identical. Far from the source, as shown in Fig. 2(c), all three methods converge as expected. Various combinations of optical properties as summarized in Table 2 were also used to test the validity of the scaling relations in SMC. The four combinations were chosen to span the range typical of soft tissues in the red or near infrared. All the results from SMC agreed very well with TMC.

In Fig. 3, the frequency domain fluence and phase were obtained for OPs: μ_a=0.20 mm^{-1} and μ_s'=0.50 mm^{-1}. Since the reduced scattering coefficient is comparable to the absorption coefficient, it is expected that the diffusion theory may not work very well even at large distances. This is evident in Fig. 3, as is the good agreement between SMC and TMC.

3.2 Effect of Finite Dimension of the Source on Fluence in Delta-P$_1$ Model

First we investigate whether the delta-P$_1$ model describes fluence better than the SDA. It has been shown[5–9] that the delta-
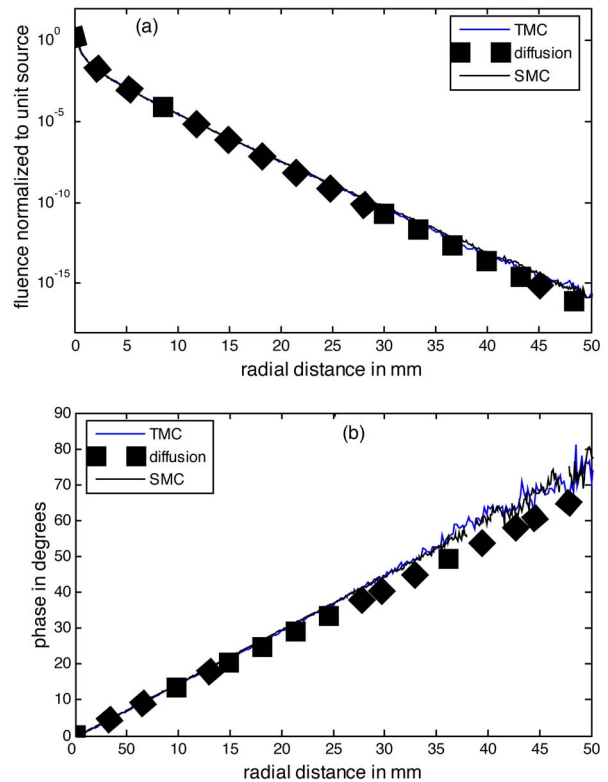

Fig. 3 Comparison of the fluence and phase in frequency domain obtained from diffusion mode (dotted line), TMC (solid line), and SMC (dashed line) versus distances for μ_a=0.20 mm^{-1}, μ_s' =0.50 mm^{-1}.
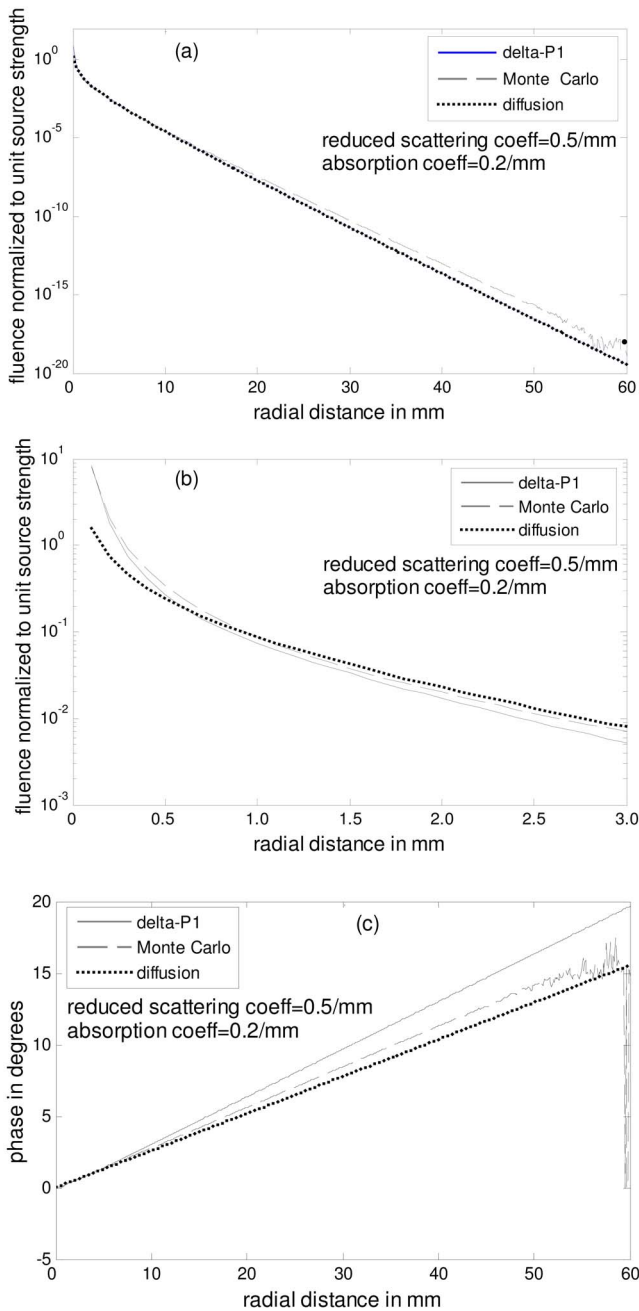
Fig. 4 (a) and (b) Fluence and (c) phase versus distance from the source. Plot (b) shows the behavior close to the source. Fluence (phase) obtained from delta-P_1 model (solid line), MC (dashed line), and diffusion model (dotted red line) as the result of OPs: μ_a =0.2 mm^{-1}, μ_s' =0.5 mm^{-1} (color online only).

P_1 model works better than the SDA in the region proximal to the source and in a transition region for a wide range of albedos. This may not be true far from the source, where the uncollided beam is negligible and diffusion dominates. The delta-P_1 model recovers Beer's law in the far region only when absorption is dominant, but when scattering is comparable to or larger than absorption, it resembles the SDA more than the true MC result. In this respect, the delta-P_1 model is most valuable in dealing with the fluence and current near the source. Figures 4(a) and 4(c) show the fluence and phase,
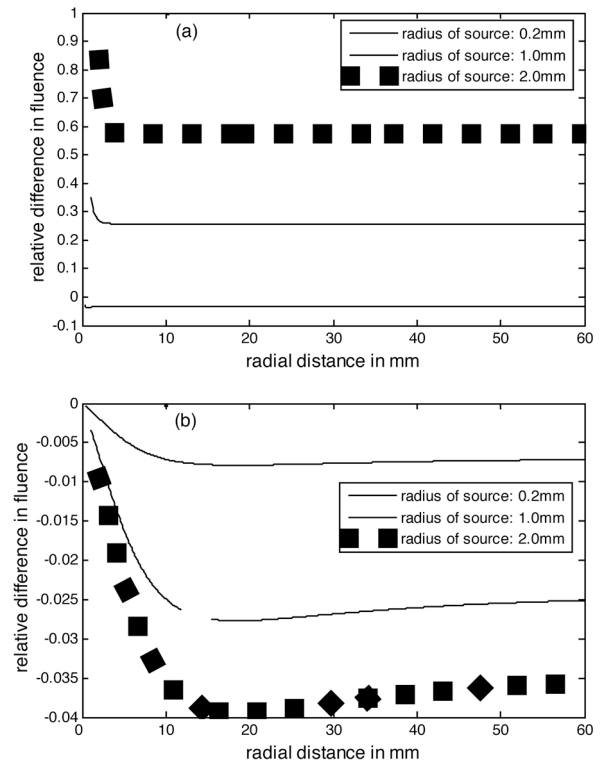

Fig. 5 Relative difference in fluence versus radial distance as obtained from the delta-P_1 model without the contribution of the second term in Eq. (23) compared with MC for different source sizes. The radii of the source spheres are 0.2, 1, and 2 mm, respectively, (a) and (b) were obtained with OPs (0.01,10,0.9) and (0.01,0.3,0.9), respectively.

respectively, as functions of distance using the delta-P_1 model, MC simulation, and the SDA for OPs: μ_a =0.2 mm^{-1} and μ_s' =0.5 mm^{-1}. The fluence plot shows that the delta-P_1 model is closer to MC than the SDA for distance less than 0.5 mm [see Fig. 4(b)]. Beyond this range, the delta-P_1 model deviates from MC and starts to resemble SDA. For the phase, the delta-P_1 model provides a worse description than SDA at all distances (including the region close to the source).

The second term in Eq. (23) represents the effect of source dimension on the fluence distribution. Two sets of OPs [(μ_a=0.01 mm^{-1}, μ_s=10.0 mm^{-1}, g=0.9) and (μ_a =0.01 mm^{-1}, μ_s=0.3 mm^{-1}, g=0.9)] were chosen to investigate how OPs affect the fluence distribution. MC simulations for each set of OPs with three source radii (0.2, 1, 2 mm) were conducted, and the fluences were compared with those calculated from the delta-P_1 model. In Fig. 5, relative differ-

Table 3 Optical properties: scattering is medium or low.

μ_s'(1/mm)	0.005	0.05	0.03	0.50	0.80	1.00
μ_a(1/mm)	0.01	0.03	0.01	0.05	0.04	0.01
μ_s'/μ_a	0.50	1.67	3.00	10.0	20.0	100.0

Table 4 Optical properties: scattering is medium or high.

$\mu_s'(1/\text{mm})$	1.00	1.50	3.00	2.00	1.00
$\mu_a(1/\text{mm})$	0.05	0.l5	0.60	0.80	0.90
μ_s'/μ_a	20.0	10.0	5.00	2.50	1.11

ence in fluence is defined as:

$$(\varphi_{\delta-p_1} - \varphi_{\delta-p_1}^w)/\varphi_{\delta-p_1}^w,$$

where $\varphi_{\delta-p_1}$ ($\varphi_{\delta-p_1}^w$) is calculated using the delta-P_1 model without (with) the contribution of the second term in Eq. (23). Hence a large relative difference indicates that the contribution of the second term is not negligible. Figure 5 shows that the relative differences obtained without and with the second term in Eq. (23) using the delta-P_1 model were negligible for both sets of OPs when the radius of the source tip was 0.2 mm or less. For the medium with higher scattering, the finite dimension of the source exerts noticeable effect on the fluence distribution as the radius increases. In the case of the medium with lower scattering, the source size does not have a significant effect on the fluence distribution, even when the radius is 2 mm. Our data (not shown here) also suggest that higher absorption tends to reduce the source size effect on the fluence.

In the following discussion, we classify the medium according to its value of reduced scattering coefficient, i.e., relatively low scattering in Table 3 and relatively high scattering in Table 4. The reason for this classification is that it appears delta-P_1 and ISM models show different fluence and phase behavior for high and low scattering media. Examining the low scattering medium, although not commonly encountered in biological tissues, allows us to thoroughly investigate various models.

3.3 *Forward Calculation Using the Delta-P_1 Model in the Frequency Domain*

Forward calculation using the delta-P_1 model was performed to describe the fluence and phase delay relative to the source.
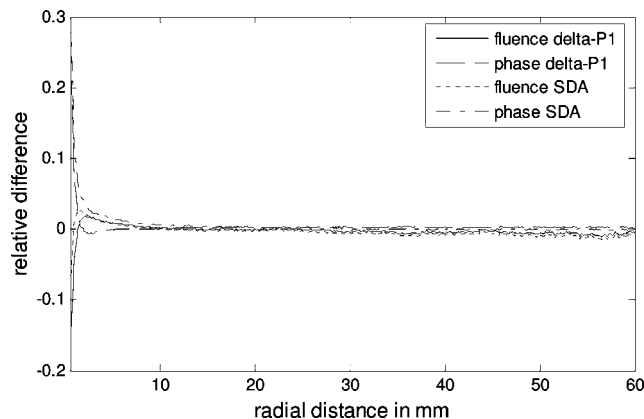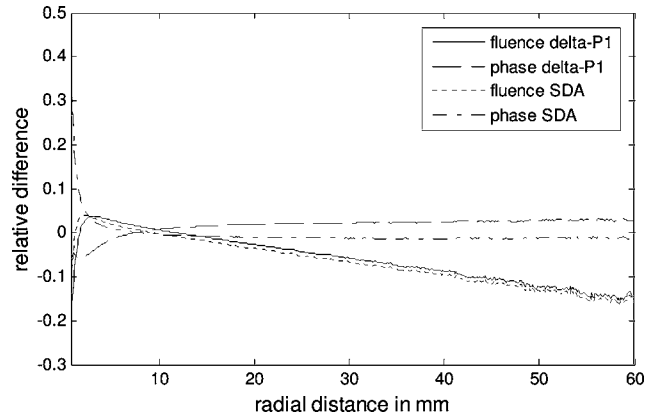

Fig. 7 Relative difference in fluence and phase calculated from SDA and delta-P_1 models compared with Monte Carlo simulation (g =0.9) as a function of position. μ_a=0.04 mm^{-1}, μ_s'=0.80 mm^{-1}.

A collection of OPs with medium and low scattering as listed in Table 3 were used. Figure 6 plots the percent relative fluence and phase difference compared with those from MC for the medium with μ_a=0.005 mm^{-1}, μ_s'=1 mm^{-1}. It demonstrates that SDA and the delta-P_1 model both describe the phase and fluence well for the region between 10 and 50 mm from the source. Closer than 10 mm, the delta-P_1 model still performs better than does SDA but gives errors up to 25% for phase and 15% for fluence. As the albedo decreases, similar results hold until the μ_s'/μ_a ratio reaches around 20, as shown in Fig. 7 for the medium with μ_a=0.04 mm^{-1} and μ_s' =0.80 mm^{-1}. The delta-P_1 model gives less than 5% error in phase for the entire region. However, the delta-P_1 model gives less than 10% error in fluence only for the region close to the source (for this albedo, less than 40 mm). It appears that the discrepancy in fluence compared to MC simulation becomes larger as the radial distance increases and grows indefinitely. The SDA shares features of the delta-P_1 model: increasing discrepancy in fluence with increasing radial distances and good prediction of phase, except in the region very close to the source. When the μ_s'/μ_a ratio is decreased to close to or less than 1, shown in Fig. 8 for the medium μ_a=0.03 mm^{-1}, μ_s'=0.05 mm^{-1}, the fluence estimated by the delta-P_1 model

Fig. 6 Relative difference in fluence and phase calculated from SDA and delta-P_1 models compared with Monte Carlo simulation (g =0.9) as a function of position. μ_a=0.005 mm^{-1}, μ_s'=1.00 mm^{-1}.
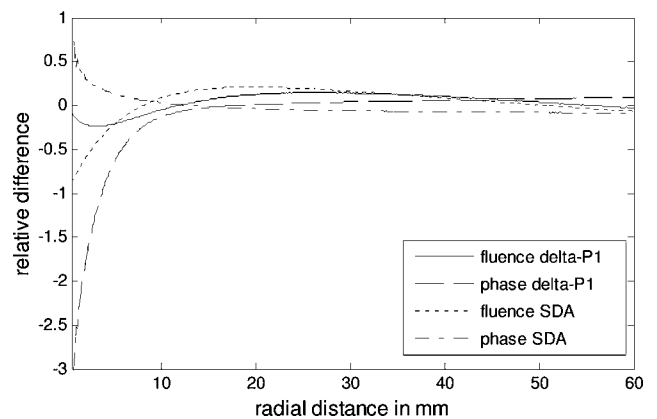

Fig. 8 Relative difference in fluence and phase calculated from SDA and delta-P_1 models compared with Monte Carlo simulation (g =0.9) as a function of position. μ_a=0.03 mm^{-1}, μ_s'=0.05 mm^{-1}.
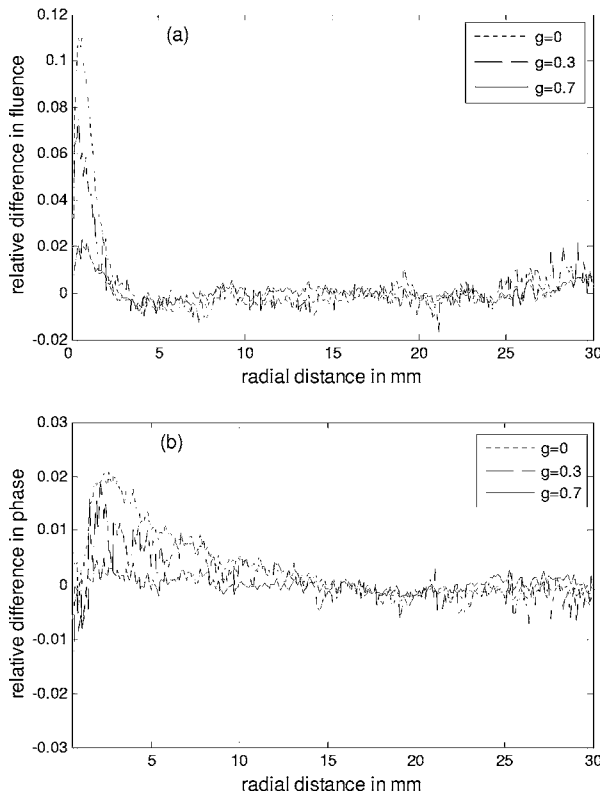
Fig. 9 Relative difference in (a) fluence and (b) phase obtained from MC using $g=0.7$ (solid line), from MC using $g=0.3$ (dashed line), and from MC using $g=0.0$ (dash-dotted line), compared with that obtained from Monte Carlo simulation ($g=0.9$) as a function of position. $\mu_a=0.01$ mm^{-1}, $\mu_s'=1.00$ mm^{-1}.

is in error by less than 25% for radial distances less than about 25 mm. SDA's description of fluence is in error by more than 25% at 5 mm and up to 85% just at the source. Hence the delta-P$_1$ model is better than SDA in terms of describing fluence close to the source for media with low albedo. The description of phase by the delta-P$_1$ model in this case is inaccurate with maximum deviation 350% close to the source, leveling off at 10% beyond 15 mm. We have plotted the absolute phase against the radial distance and discovered that the phase was negative for distance less than 4 mm. This is unphysical because it means that photons were detected prior to their being launched from the source. This is indicative of the limitations of the collimation approximation [Eq. (18)]. From the given OPs, μ_t^* can be calculated to be 0.125 mm^{-1}. The collimation approximation requires $r \geq 2/\mu_t^* = 16$ mm for the delta-P$_1$ model to be valid. Phase description by SDA is in error by less than 10% for distances greater than 15 mm. Thus for low scattering media, the delta-P$_1$ model gives a better description of fluence than SDA for low and high albedos, but the phase description is worse than that of SDA for low albedos, for all radial distances.

The preceding paragraph discussed how the delta-P$_1$ model performed for media with medium and low scattering. In reality, we often encounter biological tissues with relatively high scattering. A collection of OPs with medium and high scattering is shown in Table 4. The delta-P$_1$ model and SDA demonstrated similar trends, as shown in Fig. 7 (with μ_a
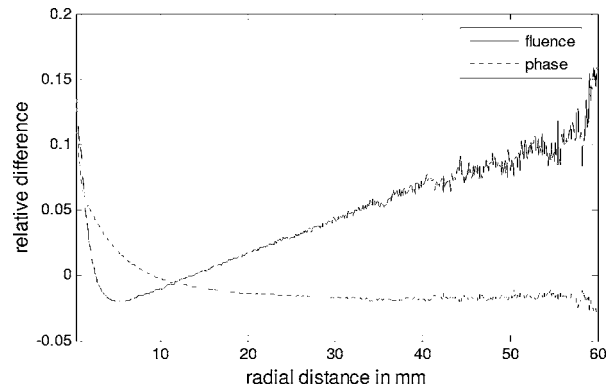

Fig. 10 Relative difference in fluence and phase obtained from ISM model compared with that obtained from Monte Carlo simulation ($g=0.9$) as a function of position. $\mu_a=0.04$ mm^{-1}, $\mu_s'=0.80$ mm^{-1}.

$=0.04$ mm^{-1} and $\mu_s'=0.80$ mm^{-1}), for $1 < \mu_s'/\mu_a < 20$, except that phase description by the delta-P$_1$ model shows improved precision compared to SDA close to the source, but a somewhat worse performance in the far region. For $\mu_s'/\mu_a > 20$, the delta-P$_1$ model rapidly converges to SDA. For high scattering media, the delta-P$_1$ model and SDA give similar descriptions of fluence for all radial distances. Phase calculated by the delta-P$_1$ model is better than that by SDA close to the source, but worse in the far region.

3.4 Forward Calculation Using the Isotropic Similarity Model in the Frequency Domain

First we used MC to investigate if the similarity relation [OPs (μ_a, μ_s, g) replaced by the equivalent OPs $(\mu_a, \mu_s', 0)$, where $\mu_s'=(1-g)\mu_s$] is a reasonable approximation for describing fluence and phase. We investigated how fluence and phase behaved if g changed from 0.9 to 0 for a fixed ratio $\mu_s'/\mu_a = 100$, where $\mu_a=0.01$ mm^{-1} and $\mu_s'=1.00$ mm^{-1}. Six chosen values of g were 0.9, 0.7, 0.5, 0.3, 0.1, and 0.0. Since the fluence ranges over several orders of magnitude, we defined the relative fluence (phase), shown in Fig. 9, as the ratio of the difference of absolute fluence (phase) from MC using $g=0.9$

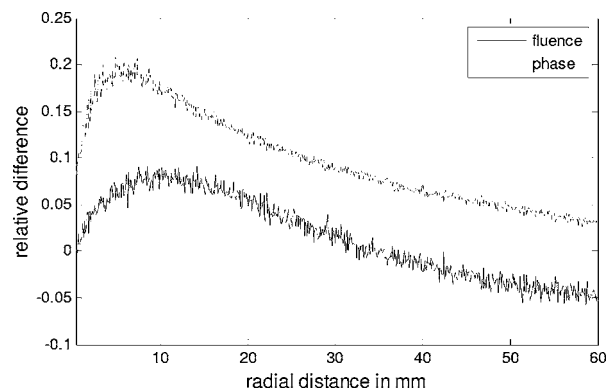

Fig. 11 Relative difference in fluence (bottom curve) and phase (top curve) obtained from ISM model compared with that obtained from Monte Carlo simulation ($g=0.9$) as a function of position. $\mu_a=0.01$ mm^{-1}, $\mu_s'=0.03$ mm^{-1}.

Table 5 Recovery of optical properties (medium and low scattering) for various μ_s'/μ_a using four models. Two positions are 4 and 9 mm from the source.

μ_s'/μ_a	Model	μ_a (1/mm)	$\mu_{a,\text{pred}}$ (1/mm)	% error	μ_s' (1/mm)	$\mu_{s,\text{pred}}'$ (1/mm)	% error
100	Diffusion	0.01	0.00980	−2.0%	1.00	0.989	−1.1%
	SMC		0.00992	−0.8%		0.990	−1.0%
	Delta-P$_1$		0.00995	−0.5%		0.979	−2.1%
	ISM		0.00986	−1.4%		0.991	−0.9%
20	Diffusion	0.04	0.0386	−3.5%	0.80	0.798	−0.3%
	SMC		0.0394	−1.5%		0.795	−0.6%
	Delta-P$_1$		0.0405	1.3%		0.767	−4.1%
	ISM		0.0388	−3.0%		0.792	−1.0%
10	Diffusion	0.05	0.0473	−5.4%	0.50	0.507	1.4%
	SMC		0.0483	−3.4%		0.511	2.2%
	Delta-P$_1$		0.0518	3.6%		0.465	−7.0%
	ISM		0.0480	−4.0%		0.507	1.4%
3	Diffusion	0.01	0.113	1030%	0.03	0.0480	60%
	SMC		0.0108	8.0%		0.0281	−6.3%
	Delta-P$_1$		0.0204	104%		0.0326	8.7%
	ISM		0.00291	−70.9%		0.0107	−64.3%
1.67	Diffusion	0.03	0.0582	94.0%	0.05	0.109	118%
	SMC		0.0268	−10.7%		0.0532	6.4%
	Delta-P$_1$		0.0653	118%		0.0961	92.2%
	ISM		0.0238	−20.7%		0.0293	−41.4%
0.5	Diffusion	0.01	0.0799	699%	0.005	0.0395	690%
	SMC		0.0109	9%		0.00489	2.2%
	Delta-P$_1$		0.0156	56.0%		0.0219	338%
	ISM		0.0087	−13.0%		0.00229	−54.2%

and that from MC using $g=0.0$ (0.3, 0.7) to the absolute fluence (phase) from MC using $g=0.9$. The maximum relative difference of fluence of 11% occurred at less than 0.5 mm from the source for $g=0$. The error rapidly dropped to less than 2% at 2 mm. Beyond that distance, the relative difference in fluence is less than 1% for all values of g. Similar behavior was observed for the relative phase, for which the maximum difference of 2% also occurred 2 mm from the source. Larger fluctuations for distances over 50 mm were due to the intrinsic noise of the MC simulations. We also examined how the relative difference in fluence and phase (percent difference in fluence obtained in the medium with $g=0.9$ and that obtained in the medium with $g=0.0$) behaved

as μ_s'/μ_a changes. Table 3 summarizes relevant optical parameters and the values of μ_s'/μ_a, which spanned more than three orders of magnitude. For $\mu_s'/\mu_a > 10$, a typical graph that demonstrates the relative difference of fluence and phase is shown in Fig. 10 for $\mu_a = 0.04$ mm^{-1}, $\mu_s' = 0.80$ mm^{-1}. The difference of phase has a maximum of 14% at the source and decreases to less than 1% beyond 5 mm. The difference in fluence is 10% at the source, rapidly decreases to 1% at about 2 mm, then gradually increases with a certain slope. However, for $\mu_s'/\mu_a > 100$, this slope is virtually zero. As μ_s'/μ_a decreases, the slope slowly increases until $\mu_s'/\mu_a = 10$, where different behavior is observed (see next). It should be noted

Table 6 Recovery of optical properties (medium and high scattering) for various μ_s'/μ_a using four models. Two positions are 3 and 6 mm from the source.

μ_s'/μ_a	Model	μ_a (1/mm)	$\mu_{a,\text{pred}}$ (1/mm)	% error	μ_s' (1/mm)	$\mu_{s,\text{pred}}'$ (1/mm)	% error
20	Diffusion	0.05	0.0483	−3.4%	1.00	0.999	−0.1%
	SMC		0.0490	−2.0%		0.998	−0.2%
	Delta-P$_1$		0.0507	1.4%		0.951	−4.9%
	ISM		0.0488	−2.4%		1.01	1.0%
10	Diffusion	0.15	0.142	−5.3%	1.50	1.52	1.3%
	SMC		0.148	−1.3%		1.52	1.3%
	Delta-P$_1$		0.157	4.7%		1.35	−10.0%
	ISM		0.145	−3.3%		1.60	6.7%
5	Diffusion	0.60	0.545	−9.1%	3.00	3.12	4.0%
	SMC		0.573	−4.5%		3.08	2.7%
	Delta-P$_1$		0.664	10.7%		2.34	−22.0%
	ISM		0.563	−6.7%		3.42	14.0%
1.11	Diffusion	0.90	0.691	−23.2%	1.00	1.23	23.0%
	SMC		0.910	1.1%		0.97	−3.0%
	Delta-P$_1$		0.960	6.7%		0.632	−36.8%
	ISM		0.946	5.1%		1.17	17.0%

that the increase is so slow that for distances of practical interest ($<$20 mm), the maximum error in fluence is only a few percent. It appears that the relative errors for phase are smaller than those for fluence for high scattering coefficients. Figure 11 plotted with $\mu_a=0.01$ mm^{-1} and $\mu_s'=0.03$ mm^{-1} shows the typical trend for the relative differences of fluence and phase when $0.5<\mu_s'/\mu_a<10$. The difference in phase reaches its maximum value at about 5 mm and gradually decreases away from the source. The difference of fluence reaches its maximum value at about 9 mm and also gradually decreases with distance. It is interesting to note that for this domain, the relative errors in phase exceed those in fluence, just the opposite to the conclusion drawn for media with high albedo.

Having explored the validity of the similarity relationships using MC, we then performed analytical calculations using Eq. (37) to obtain the amplitude and phase of the complex fluence for a number of OPs whose μ_s'/μ_a ratios range from 1 to 100. It was found that the fluence amplitude calculated from the ISM model agreed with that obtained from MC (g =0.0) for all these OPs across the distances investigated (0.1 to 60 mm) with less than 0.5% error. However, the estimate of the phase using the analytical expressions was less satisfactory, agreeing well closer to the source but deviating from MC in the far region for relatively high μ_s'. This supports the claim that the coefficient in the second-order term in Eq. (35)

does play a role in estimating the phase. We also performed a numerical calculation of Eq. (33) using the double exponential formula. It was found that both analytical and numerical methods gave satisfactory descriptions of fluence and phase within 10 mm for all OPs listed in Tables 3 and 4. The fluence and phase calculated by the analytical solution start to deviate from those of the numerical method beyond 10 mm when $\mu_s'>0.3$ mm^{-1} (μ_a is usually less than μ_s'). To be cautious, numerical integration was invoked for this range of OPs.

3.5 Inverse Calculation Using Four Models

Since we are interested in interstitial detection of light, detector locations are typically less than 1 cm from the source. In this work, two detector locations were chosen to be 4 and 9 mm for low absorption media as shown in Table 5, and 3 and 6 mm for high absorption media as shown in Table 6. Shorter distances were chosen for high absorption media because the signal becomes virtually undetectable in practice. For medium and low scattering media, recovery of reduced scattering and absorption coefficients is within 5% for μ_s'/μ_a greater than 10 for all models (Table 5). When μ_s'/μ_a is less than 10, the SDA and delta-P$_1$ models break down completely, because SDA cannot give good estimates of fluence, and delta-P$_1$ is unable to give correct phase values. The ISM model fares better, with the estimate of μ_a within 70% and μ_s'

Table 7 Recovered OPs when noise was added to phase and amplitude of 5% (second row), 10% (third row), and the fixed 0.5 deg in phase and amplitude at the origin divided 100 (fourth row). The expected OPs: $\mu_s' = 1.00$ mm^{-1}, $\mu_a = 0.01$ mm^{-1}. Data were taken at 4- and 9-mm positions. The numbers in brackets are relative errors.

Noise added	Optical properties	Diffusion	SMC	Delta-P$_1$	ISM
5% of the phase and amplitude	μ_a mm^{-1}	9.73×10^{-3} (4.9%)	9.90×10^{-3} (4.2%)	9.74×10^{-3} (4.9%)	9.83×10^{-3} (5.1%)
	μ_s' mm^{-1}	9.78×10^{-2} (4.8%)	9.86×10^{-2} (5.3%)	9.78×10^{-2} (5.5%)	9.67×10^{-2} (5.0%)
10% of the phase and amplitude	μ_a mm^{-1}	9.69×10^{-3} (13.5%)	9.72×10^{-3} (12.8%)	9.79×10^{-3} (14.1%)	9.90×10^{-3} (14.1%)
	μ_s' mm^{-1}	9.94×10^{-2} (12.1%)	9.87×10^{-2} (13.4%)	9.61×10^{-2} (13.4%)	9.68×10^{-2} (13.1%)
0.5 deg in phase (amplitude/100) at the origin	μ_a mm^{-1}	9.84×10^{-3} (7.3%)	9.92×10^{-3} (7.0%)	9.95×10^{-3} (7.5%)	9.86×10^{-3} (6.8%)
	μ_s' mm^{-1}	9.89×10^{-2} (6.7%)	9.89×10^{-2} (6.2%)	9.79×10^{-2} (6.4%)	9.91×10^{-2} (7.8%)

within 64%. This suggests that even though the difference of fluence and phase is within 20%, the inverse calculation still gives fairly large errors in recovering OPs. Hence, inverse calculation is sensitive to the small variations of fluence and phase. For medium and high scattering media, all four models perform very well for μ_s'/μ_a greater than 10. When the albedo is decreased, SDA gives a maximum error of about 25% for μ_s'/μ_a as low as 1.11. The ISM model gives 17% error of the estimate of μ_s' and 5.1% error of the estimate of μ_a. The delta-P$_1$ model performs slightly better than diffusion theory but worse than the ISM. It is not surprising that the SMC model works very well for all types of media, since no approximation has been used in the forward calculation (small deviations are due to interpolation errors). It is generally thought that SDA does not perform well if μ_s'/μ_a is not large, but from our results, the inverse calculation using SDA as a forward model can recover μ_s' and μ_a both within 10% for μ_s'/μ_a as low as 5. It can also be seen that SDA does not apply well for distances within several mean free paths, as shown in Table 5. Fortunately, most biological tissues have scattering coefficients greater than 0.5 mm^{-1}. Hence, diffusion theory should be adequate in most practical circumstances. It is interesting to note that the delta-P$_1$ model behaves about the same as the diffusion theory in recovering OPs, in contrast to findings in other papers. The discrepancy may be due to the fact that: 1. the collimation approximation is not good enough for a point source; and 2. the measured quantity in our case is fluence instead of irradiance. For the latter, since the fluence is the integral of the radiance over 4π while the irradiance is the integral over some forward solid angle, it is likely that the delta-P$_1$ model may provide a more accurate description of the radiance in the forward direction. Hence, although improvement over SDA has been reported for irradiance,[7,8,23] this may not be true for fluence.

Using the Box-Muller method, Gaussian distributed noise has been added to the amplitude ratio and the phase to simulate the signal-to-noise ratio in the actual measurements. The robustness of the inversion scheme has been tested by adding noise proportional to the signal or of a fixed amplitude. For proportional noise, standard deviations of 5 and 10% were used. For fixed amplitude, the standard deviation was 0.5 deg in phase and the fluence at the origin divided by 100. These values were based on typical experimental uncertainties. In Table 7, the ratio of the standard deviation in the recovered optical coefficients divided by the mean is approximately 5% at 5% noise added. This ratio increased to about 13% when 10% noise was added. For the fixed added noise, the ratio is about 7%.

There is potential for improving ISM model performance for medium and high scattering media, since the fluence error displays a set behavior and the phase error is not large. If we can find the minimum of the fluence difference curve and its slope beyond the position where the minimum occurs (see Fig. 10, for example), the fluence in the anisotropic medium could then be modified accordingly. This requires a look-up table to store the relevant conditions and may not give any advantage compared to the SMC model.

It is interesting to note that ISM consistently gives better estimates of μ_a than of μ_s' (for medium and high scattering media, it can recover μ_a within 5% for μ_s'/μ_a as low as 1), while SDA tends to recover μ_s' better than μ_a. The latter observation was also noted in the thesis by Boas.[34] Hence the combination of ISM (estimating μ_a) and SDA (estimating μ_s') will definitely provide better estimates of OPs than using either model alone.

The major inconvenience for using SMC is that for a particular set of reference data, OPs that can be accessed in the search parameter space are limited to a certain range because of the scaling effect. A possible way to alleviate this problem is to use diffusion theory and the ISM model to obtain rough estimates of OPs, then the SMC to refine the results. This is only necessary for media with low albedo, since combined diffusion theory and ISM is sufficiently accurate (within 5 to 10% for μ_s'/μ_a as low as 5) to recover OPs for media with high albedo.

4 Conclusion

In this study, inverse calculation to determine absorption and reduced scattering coefficients is conducted using the following four models: standard diffusion theory (SDA), single Monte Carlo (SMC), delta-P_1, and isotropic similarity (ISM) in the frequency domain. Fluence and phase, which were used as input parameters to the inversion algorithm, were generated from Monte Carlo simulation in an infinite medium with an isotropic source situated at the origin. To simulate interstitial photodynamic therapy protocols, fluence and phase data within 10 mm of the source were used. We show that SMC is the best model of the four, being able to recover OPs within 10% error for media with all the albedos investigated. Diffusion theory recovers OPs for media with $\mu_s'/\mu_a > 10$ within 10% error, but is unsatisfactory for media with $\mu_s'/\mu_a < 10$. The delta-P_1 model offers no real advantage over diffusion theory for all values of OPs investigated. Possible reasons may be the breakdown of the collimation approximation and/or the use of fluence instead of irradiance. ISM generally works no worse than SDA with some improvement in recovering μ_a for media with relatively high scattering, which is typical of biological tissues. This study demonstrates that combined diffusion theory and ISM is adequate for the recovery of OPs (within 5 to 10%) for most biological tissues (as long as $\mu_s'/\mu_a > 5$). If *a priori* knowledge of OPs is unavailable, the possible range of the OPs may be obtained by diffusion theory, followed by the use of the SMC model for improved accuracy.

5 Appendix A

Here we derive the SMC formula in the frequency domain (FD). By definition, the FD fluence is:

$$\widetilde{\phi}(\omega, r) = \int_0^\infty \phi(t, r)\exp(i\omega t)dt. \tag{38}$$

To evaluate this integral, we have to discretize the time axis. Thus the previous equation becomes:

$$\widetilde{\phi}(\omega, r) = \sum_{k=0}^\infty \phi(t_k, r)\exp(i\omega t)\Delta t_k. \tag{39}$$

Note that:

$$\phi(t, r) = \phi\left(\frac{\mu_{tn}}{\mu_t}t, \frac{\mu_{tn}}{\mu_t}r\right). \tag{40}$$

We can choose $t_k = \mu_{tn}/\mu_t t_l$, where t_l is the discretization of time axis for the unscaled fluence $\phi(t, r)$ to avoid interpolating values of $\phi(t, r)$. We have:

$$\widetilde{\phi}(\omega, r) = \sum_{k=0}^\infty \phi(t_k, r)\exp(i\omega t_k)\Delta t_k$$

$$= \sum_{k=0}^\infty \phi\left(\frac{\mu_{tn}}{\mu_t}t_l, r\right)\exp\left(i\omega\frac{\mu_{tn}}{\mu_t}t_l\right)\frac{\mu_{tn}}{\mu_t}\Delta t_l$$

$$= \sum_{k=0}^\infty \phi(t_l, r)\exp\left(i\omega\frac{\mu_{tn}}{\mu_t}t_l\right)\frac{\mu_{tn}}{\mu_t}\Delta t_l. \tag{41}$$

In practice, t_l and Δt_l are usually chosen to be 1 psec.

6 Appendix B

In steady state, the modulation frequency is zero. Equation (22) is simplified to:

$$(\nabla^2 - 3\mu_a\mu_t')\varphi_d(\vec{r}, \omega) = -3\mu_s^*\mu_t' P(\vec{r}, \hat{s}_0) + 3g^*\mu_s^*\hat{s}_0 \cdot \nabla P(\vec{r}, \hat{s}_0), \tag{42}$$

with boundary conditions:

$$\varphi_d(\vec{r}) - Ah\hat{r} \cdot \nabla \varphi_d(\vec{r}) = \frac{-3Ahg^*\mu_s^*}{4\pi r_0^2}, \tag{43}$$

$$\varphi_d(r) \rightarrow 0 \quad \text{for } r \rightarrow \infty. \tag{44}$$

We are going to solve for Green's function associated with Eqs. (42)–(44).

$$(\nabla^2 - \mu_{\text{eff}}^2)G(\vec{r}, \vec{r}') = -\delta(\vec{r} - \vec{r}'),$$

$$[G(\vec{r}, \vec{r}') - Ah\vec{r}_0 \cdot \nabla G(\vec{r}, \vec{r}')]\big|_{r=r_0} = 0, \tag{45}$$

$$G(\vec{r}, \vec{r}') \rightarrow 0, \quad \text{as } r \rightarrow \infty. \tag{46}$$

Let $G(\vec{r}, \vec{r}') = U(\vec{r}, \vec{r}') + V(\vec{r}, \vec{r}')$ such that

$$(\nabla^2 - \mu_{\text{eff}}^2)U(\vec{r}, \vec{r}') = -\delta(\vec{r} - \vec{r}'), \tag{47}$$

$$U(\vec{r}, \vec{r}') \rightarrow 0, \quad \text{as } r \rightarrow \infty, \tag{48}$$

and

$$(\nabla^2 - \mu_{\text{eff}}^2)V(\vec{r}, \vec{r}') = -\delta(\vec{r}, \vec{r}'),$$

$$[V(\vec{r}, \vec{r}') - Ah\vec{r}_0 \cdot \nabla V(\vec{r}, \vec{r}')]\big|_{r=r_0}$$
$$= -[U(\vec{r}, \vec{r}') - Ah\vec{r}_0 \cdot \nabla U(\vec{r}, \vec{r}')]\big|_{r=r_0}, \tag{49}$$

$$V(\vec{r}, \vec{r}') \rightarrow 0, \quad \text{as } r \rightarrow \infty. \tag{50}$$

The solution for $U(\vec{r}, \vec{r}')$ can be readily found to be:

$$U(\vec{r}, \vec{r}') = \frac{\exp(-\mu_{\text{eff}}|\vec{r} - \vec{r}'|)}{4\pi|\vec{r} - \vec{r}'|}. \tag{51}$$

This can also be expressed in a form suitable for use with spherical coordinates by using the addition theorem for Bessel functions:

$$U(\vec{r},\vec{r}') = \frac{1}{4\pi\sqrt{rr'}}\sum_{n=0}^{\infty}(2n+1)K_{n+\frac{1}{2}}(\mu_{\text{eff}}r')$$

$$\times I_{n+\frac{1}{2}}(\mu_{\text{eff}}r)P_n(\cos\theta), \quad \text{for } r < r', \quad (52)$$

$$U(\vec{r},\vec{r}') = \frac{1}{4\pi\sqrt{rr'}}\sum_{n=0}^{\infty}(2n+1)K_{n+\frac{1}{2}}(\mu_{\text{eff}}r)$$

$$\times I_{n+\frac{1}{2}}(\mu_{\text{eff}}r')P_n(\cos\theta), \quad \text{for } r > r', \quad (53)$$

where I and K are modified Bessel functions of the first and second kind, respectively. The solution of $V(\vec{r},\vec{r}')$ can be written as the following infinite sum:

$$V(r,\theta,r') = \sum_{n=0}^{\infty}C_n(r')r^{-\frac{1}{2}}K_{n+\frac{1}{2}}(\mu_{\text{eff}}r)P_n(\cos\theta). \quad (54)$$

The $C_n(r')$ are determined by the boundary conditions of Eqs. (49) and (50).

$$C_n(r') = -\frac{2n+1}{4\pi\sqrt{r'}}K_{n+\frac{1}{2}}(\mu_{\text{eff}}r')$$

$$\times\frac{I_{n+1/2}(\mu_{\text{eff}}r_0)/\sqrt{r_0} - Ah[I_{n+1/2}(\mu_{\text{eff}}r)/\sqrt{r}]'|_{r=r_0}}{K_{n+1/2}(\mu_{\text{eff}}r_0)/\sqrt{r_0} - Ah[K_{n+1/2}(\mu_{\text{eff}}r)/\sqrt{r}]'|_{r=r_0}}. \quad (55)$$

In particular,

$$C_0 = -\frac{1}{4\pi}\frac{K_{1/2}(\mu_{\text{eff}}r')}{\sqrt{r'}}\widetilde{C}_0, \quad (56)$$

where

$$\widetilde{C}_0 = \frac{I_{1/2}(\mu_{\text{eff}}r_0) - Ah\mu_{\text{eff}}I_{3/2}(\mu_{\text{eff}}r_0)}{K_{1/2}(\mu_{\text{eff}}r_0) - Ah\mu_{\text{eff}}K_{3/2}(\mu_{\text{eff}}r_0)}. \quad (57)$$

Hence Green's function for our geometry is:

$$G(\vec{r},\vec{r}') = \frac{\exp(-\mu_{\text{eff}}|\vec{r}-\vec{r}'|)}{4\pi|\vec{r}-\vec{r}'|}$$

$$+\sum_{n=0}^{\infty}C_n r^{-1/2}K_{n+1/2}(\mu_{\text{eff}}r)P_n(\cos\theta). \quad (58)$$

Green's second identity allows us to obtain the solution for the fluence.

$$\varphi_d(r) = 3\mu_s^*(\mu_t^* + g^*\mu_a)\int_{V'}G(\vec{r},\vec{r}')P(r')dV'$$

$$-3g^*\mu_s^*\int_{r'=r_0}G(\vec{r},\vec{r}')P(r')dS'. \quad (59)$$

By substituting Green's function in Eq. (58) into Eq. (59), we obtain Eqs. (23)–(25).

7 Appendix C

Direct use of a residue theorem to evaluate the integral in Eq. (37) is complicated, since it involves double poles. However, we used the following method to reduce the double pole to a simple pole. Define an auxiliary integral $F_{\text{aux}}(r)$ as:

$$F_{\text{aux}}(r) = \frac{1}{2\pi i}\int_{-\infty}^{+\infty}\frac{k}{k^2+1}\cdot\frac{\exp(ik\mu_t'r)}{[1-(c/k)\cdot\tan^{-1}k]}dk. \quad (60)$$

It can be shown by simple calculation that

$$F(r) = F_{\text{aux}}(r) + c\frac{\partial F_{\text{aux}}(r)}{\partial c}. \quad (61)$$

The problem reduces to evaluation of the integral $F_{\text{aux}}(r)$. The residue theorem still cannot be applied directly to evaluate $F_{\text{aux}}(r)$, since the branch point and one of the poles coincide. To get around this difficulty, we multiply the pole at i by δ, where δ is less than but extremely close to one. Then, we have

$$F_{\text{aux}}(r,\delta) = \frac{1}{2\pi i}\int_{-\infty}^{+\infty}\frac{k}{k^2\delta^2+1}\cdot\frac{\exp(ik\mu_t'r)}{[1-(c/k)\cdot\tan^{-1}k]}dk. \quad (62)$$

In the end, the limit $\delta\to1$ restores the value of $F(r)$. We separate $F_{\text{aux}}(r,\delta)$ into two easier integrals:

$$F_{\text{aux}}(r,\delta) = -\frac{1}{2\delta}\left[\frac{1}{2\pi}\int_{-\infty}^{+\infty}\frac{1}{1-ik\delta}\cdot\frac{\exp(ik\mu_t'r)}{1-(c/k)\cdot\tan^{-1}k}dk\right.$$

$$\left.-\frac{1}{2\pi}\int_{-\infty}^{+\infty}\frac{1}{1+ik\delta}\cdot\frac{\exp(ik\mu_t'r)}{1-(c/k)\cdot\tan^{-1}k}dk\right]. \quad (63)$$

By applying the results in Appendix D in Case, deHoffmann and Placzek,[31] the two integrals (the first and the second are denoted by I_1 and I_2, respectively) can be evaluated as:

$$I_1 = -c\frac{\partial a_0}{\partial c}\frac{\exp(-a_0\mu_t'r)}{1+a_0\delta} + \frac{c}{2}\int_0^1\frac{g(c,\xi)}{\xi+1}\exp(-\mu_t'r/\xi)d\xi, \quad (64)$$

$$I_2 = -c\frac{\partial a_0}{\partial c}\frac{\exp(-a_0\mu_t'r)}{1-a_0} + \frac{c}{2}VP\int_0^1\frac{g(c,\xi)}{\xi-\delta}\exp(-\mu_t'r/\xi)d\xi$$

$$+\exp(-\mu_t'r)g(c,\delta)(1-c\tanh^{-1}\delta). \quad (65)$$

The limit $\delta\to1$ has been taken wherever allowed. The VP stands for the Cauchy principal value. Although the form of the solution may not look simple, it is easy to implement on a computer.

References

1. S. R. Arridge, "Photon measurement density functions. Part I: Analytical forms," *Appl. Opt.* **34**, 7395–7409 (1995).
2. S. R. Arridge and M. Schweiger, "Photon measurement density functions. Part II: Finite-element-method calculations," *Appl. Opt.* **34**, 8026–8037 (1995).
3. M. S. Patterson, B. Chance, and B. C. Wilson, "Time resolved reflectance and transmittance for the noninvasive measurement of tissue optical properties," *Appl. Opt.* **28**, 2331–2336 (1989).
4. T. J. Farrell, M. S. Patterson, and B. C. Wilson "A diffusion theory model of spatially resolved, steady-state diffuse reflectance for the noninvasive determination of tissue optical properties *in vivo*," *Med. Phys.* **19**(4), 879–888 (1992).
5. S. A. Prahl, "Light transport in tissue," PhD Thesis, University of Texas at Austin, Austin, TX (1988).
6. W. M. Star, "Diffusion theory of light transport," Chap. 6 in *Optical-Thermal Response of Laser-Irradiated Tissue*, A. J. Welch and M. J. van Gemert, Eds., pp. 131–206, Plenum Press, New York (1995).
7. V. Venugopalan, J. S. You, and B. J. Tromberg, "Radiative transport in the diffusion approximation: An extension for highly absorbing media and small source-detector separations," *Phys. Rev. E* **58**, 2395–2407 (1998).
8. S. A. Carp, S. A. Prahl, and V. Venugopalan, "Radiative transport in the delta-P_1 approximation: Accuracy of fluence rate and optical penetration depth predictions in turbid semi-infinite media," *J. Biomed. Opt.* **9**(3), 632–647 (2004).
9. J. S. You, C. K. Hayakawa, and V. Venugopalan, "Delta-P_1 approximation to radiative transport in the frequency domain," *Phys. Rev. E* **72**(2), 021903 (2005).
10. L. T. Perelman, J. Winn, J. Wu, R. R. Dasari, and M. S. Feld, "Photon migration of near-diffusive photons in turbid media: A Lagrangian-based approach," *J. Opt. Soc. Am. A* **14**(1), 224–229 (1997).
11. S. L. Jacques and L. Wang, "Monte Carlo modeling of light transport in tissues," Chap. 4 in *Optical-Thermal Response of Laser-Irradiated Tissue*, A. J. Welch and M. J. van Gemert, Eds., pp. 73–100, Plenum Press, New York (1995).
12. R. F. Bonner, R. Nossal, S. Havlin, and G. H. Weiss, "Model for photon migration in turbid biological media," *J. Opt. Soc. Am. A* **4**, 423–432 (1987).
13. A. H. Gandjbakhche, R. Nossal, and R. F. Bonner, "Scaling relationships for theories of anisotropic random walks applied to tissue optics," *Appl. Opt.* **32**, 504–516 (1993).
14. A. Kienle and M. S. Patterson, "Determination of the optical properties of semi-infinite turbid media from frequency-domain reflectance close to the source," *Phys. Med. Biol.* **42**, 1801–1819 (1997).
15. A. Kienle and M. S. Patterson, "Determination of the optical properties of turbid media from a single Monte Carlo simulation," *Phys. Med. Biol.* **41**, 2221–2227 (1996).
16. A. Pifferi, P. Taroni, G. Valentini, and S. Andersson-Engels, "Real-time method for fitting time-resolved reflectance and transmittance measurements with a Monte Carlo model," *Appl. Opt.* **37**, 2774–2780 (1998).
17. J. B. Fishkin, P. T. C. So, A. E. Cerussi, S. Fantini, M. A. Franceschini, and E. Gratton, "Frequency-domain method for measuring spectral properties in multiple-scattering media: Methemoglobin absorption spectrum in a tissuelike phantom," *Appl. Opt.* **34**, 1143–1155 (1995).
18. T. H. Pham, T. Spott, L. O. Svaasand, and B. J. Tromberg, "Quantifying the properties of two-layer turbid media with frequency-domain diffuse reflectance," *Appl. Opt.* **39**, 4733–4745 (2000).
19. X. D. Li, M. A. O'Leary, D. A. Boas, B. Chance, and A. G. Yodh, "Fluorescence diffuse photon density waves in homogeneous and heterogeneous turbid media: Analytical solutions and applications," *Appl. Opt.* **35**, 3746–3758 (1996).
20. R. Graaff, M. H. Koelink, F. F. M. de Mul, W. G. Zijlstra, A. C. M. Dassel, and J. G. Aarnoudse, "Condensed Monte Carlo simulations for the description of light transport," *Appl. Opt.* **32**, 426–434 (1993).
21. A. Sassaroli, C. Blumetti, F. Martelli, L. Alianelli, D. Contini, A. Ismaelli, and G. Zaccanti, "Monte Carlo procedure for investigating light propagation and imaging of highly scattering media," *Appl. Opt.* **37**, 7392–7400 (1998).
22. C. K. Hayakawa, J. Spanier, F. Bevilacqua, A. K. Dunn, J. S. You, B. J. Tromberg, and V. Venugopalan, "Perturbation Monte Carlo methods to solve inverse photon migration problems in heterogeneous tissues," *Opt. Lett.* **26**, 1335–1337 (2001).
23. C. K. Hayakawa, B. Y. Hill, J. S. You, F. Bevilacqua, J. Spanier, and V. Venugopalan, "Use of the δ-P_i approximation for recovery of optical absorption, scattering, and asymmetry coefficients in turbid media," *Appl. Opt.* **43**, 4677–4684 (2004).
24. D. R. Wyman, M. S. Patterson, and B. C. Wilson, "Similarity relations for anisotropic scattering in Monte Carlo simulations of deeply penetrating neutral particles," *J. Comput. Phys.* **81**, 137–150 (1989).
25. H. C. van de Hulst and K. Grossman, "Multiple light scattering in planetary atmosphere" in *The Amospheres of Venus and Mars*, J. C. Brandt and M. B. McElroy, Eds., pp. 35, Gordon and Breach, New York (1968).
26. D. R. Wyman, M. S. Patterson, and B. C. Wilson, "Similarity relations for the interaction parameters in radiation transport," *Appl. Opt.* **28**, 5243–5249 (1989).
27. W. M. Star, J. P. A. Marijnissen, and M. J. C. van Gemert, "Light dosimetry in optical phantoms and in tissues: I. Multiple flux and transport theory," *Phys. Med. Biol.* **33**, 437–454 (1988).
28. R. Graaff, J. G. Aarnoudse, F. F. M. de Mul, and H. W. Jentink, "Similarity relations for anisotropic scattering in absorbing media," *Opt. Eng.* **32**(2), 244–252 (1993).
29. H. C. van de Hulst and R. Graaff, "Aspects of similarity in tissue optics with strong forward scattering," *Phys. Med. Biol.* **41**, 2519–2531 (1996).
30. W. J. Wiscombe "The delta-M method: Rapid yet accurate radiative flux calculations for strongly asymmetric phase functions," *J. Atmos. Sci.* **34**, 1408–1422 (1977).
31. K. M. Case, F. de Hoffmann, and G. Placzek, *Introduction to the Theory of Neutron Diffusion*, Los Alamos Scientific Laboratory, Los Alamos, NM (1953).
32. T. Ooura and M. Mori, "A robust double exponential formula for Fourier-type integrals," *J. Comput. Appl. Math.* **112**, 229–241 (1999).
33. P. R. Bevington and D. K. Robinson, *Data Reduction and Error Analysis for the Physical Sciences*, 2nd ed., McGraw-Hill, Inc. (1992).
34. D. A. Boas, "Diffusion photon probes of structural and dynamical properties of turbid media: theory and biomedical applications," PhD Thesis, Univ. of Pennsylvania (1996).